AFRL-OSR-VA-TR-2014-0310

PHYSICS-BASED COMPUTATIONAL ALGORITHM FOR THE MULTIFLUID PLASMA MODEL

Uri Shumlak
UNIVERSITY OF WASHINGTON

10/29/2014
Final Report

Air Force Research Laboratory
AF Office Of Scientific Research (AFOSR)/ RTA
Arlington, Virginia 22203
Air Force Materiel Command

REPORT DOCUMENTATION PAGE

Form Approved
OMB No. 0704-0188

1. REPORT DATE *(DD-MM-YYYY)*	**2. REPORT TYPE**	**3. DATES COVERED** *(From - To)*
30-06-2014	Final	01-07-2011 to 30-06-2014

4. TITLE AND SUBTITLE

Physics-Based Computational Algorithm for the Multi-Fluid Plasma Model

5a. CONTRACT NUMBER
FA9550-11-1-0167

5b. GRANT NUMBER
FA9550-11-1-0167

5c. PROGRAM ELEMENT NUMBER

6. AUTHOR(S)
Uri Shumlak

5d. PROJECT NUMBER

5e. TASK NUMBER

5f. WORK UNIT NUMBER

7. PERFORMING ORGANIZATION NAME(S) AND ADDRESS(ES)
University of Washington
Aerospace & Energetics Research Program
Box 352250
Seattle, WA 98195-2250

8. PERFORMING ORGANIZATION REPORT NUMBER

9. SPONSORING / MONITORING AGENCY NAME(S) AND ADDRESS(ES)

Dr. Fariba Fahroo
Program Manager, Computational Mathematics
AFOSR/NL
875 N. Randolph St. Rm 3112

10. SPONSOR/MONITOR'S ACRONYM(S)

11. SPONSOR/MONITOR'S REPORT NUMBER(S)

12. DISTRIBUTION / AVAILABILITY STATEMENT

Approved for public release

13. SUPPLEMENTARY NOTES

14. ABSTRACT

A physics-based algorithm is developed based on the multi-fluid plasma model derived from moments of the Boltzmann equation. The model includes evolution equations for the electromagnetic fields, electron fluid, ion fluid, neutral fluid, and any additional species. The characteristic time scales for the electromagnetic fields is much shorter than the time scales of the ion and neutral fluids. The physics-based computational algorithm solves fluid models for each plasma species that are appropriate for the expected physical behavior. The numerical discretization is developed specifically to capture the expected physical behavior by combining high-order continuous and discontinuous spatial representations of the solution and implicit time-advance methods to accurately capture the fast and slow dynamics. The physics-based computational algorithm has also been extended to solving continuum kinetic plasma models. Solving Maxwell's equations has been improved by using a parabolic modification to ensure the errors of divergence constraint equations are properly removed and handled. Nonreflecting boundary conditions using a lacunae-based method have been implemented and provide higher solution fidelity for open boundary problems.

15. SUBJECT TERMS

advanced plasma models, high-order algorithms, multiscale physics, mathematically stiff equations

16. SECURITY CLASSIFICATION OF:			**17. LIMITATION OF ABSTRACT**	**18. NUMBER OF PAGES**	**19a. NAME OF RESPONSIBLE PERSON**
a. REPORT	**b. ABSTRACT**	**c. THIS PAGE**			Uri Shumlak
U	U	U	UU	31	**19b. TELEPHONE NUMBER** *(include area code)* 206-616-1986

Standard Form 298 (Rev. 8-98)
Prescribed by ANSI Std. Z39.18

Final Performance Report (7/1/11 – 6/30/14)

AFOSR Grant No. FA9550-11-1-0167

"PHYSICS-BASED COMPUTATIONAL ALGORITHM FOR THE MULTI-FLUID PLASMA MODEL"

Submitted to

Dr. Fariba Fahroo
Program Manager, Computational Mathematics
Air Force Office of Scientific Research / NL
875 N. Randolph St, Rm 3112
Arlington, VA 22203

University of Washington
Department of Aeronautics and Astronautics
Aerospace & Energetics Research Program
Box 352250
Seattle, WA 98195-2250

Dr. Uri Shumlak
Principal Investigator

9/30/14

PHYSICS-BASED COMPUTATIONAL ALGORITHM FOR THE MULTI-FLUID PLASMA MODEL

AFOSR Grant No. FA9550-11-1-0167

U. Shumlak

Department of Aeronautics and Astronautics
Aerospace & Energetics Research Program
University of Washington

Abstract

A physics-based algorithm is developed based on the multi-fluid plasma model derived from moments of the Boltzmann equation. The model includes evolution equations for the electromagnetic fields, electron fluid, ion fluid, neutral fluid, and any additional species. The large mass difference between electrons and ions introduces disparate time and spatial scales and requires a numerical algorithm with sufficient accuracy to capture the multiple scales. In addition, the characteristic time scales for the electromagnetic fields is much shorter than the time scales of the ion and neutral fluids. The physics-based computational algorithm solves fluid models for each plasma species that are appropriate for the expected physical behavior, by combining $5N$-moment and $13N$-moment fluid models for multicomponent plasmas. The numerical discretization is developed specifically to capture the expected physical behavior by combining high-order continuous and discontinuous spatial representations of the solution and implicit time-advance methods to accurately capture the fast and slow dynamics. The physics-based computational algorithm has also been extended to solving continuum kinetic plasma models. Solving Maxwell's equations has been improved by using a parabolic modification to ensure the errors of divergence constraint equations are properly removed and handled. Nonreflecting boundary conditions using a lacunae-based method have been implemented and provide higher solution fidelity for open boundary problems.

1 Project Description

Plasmas are essential to many existing and emerging technologies that are important to the Air Force, industry, and general science. These applications include high power microwave devices, plasma actuation of airstreams, drag reduction for hypersonic vehicles, advanced space propulsion, weapons effects simulations, radiation production from

fusion, etc. Advancing plasma technologies requires a fundamental and accurate understanding of the underlying physical effects and the resulting plasma dynamics. Plasma dynamics inherently involve complex physical phenomena because the dynamics are affected by short-range (collisions) and long-range (electromagnetic fields) forces. The great utility of plasmas stems from these multi-scale forces. In general, plasmas fall into a density regime where they exhibit both collective (fluid) behavior and individual (particle) behavior. The intermediate regime complicates the analytical and computational modeling of plasmas. Accurate computational modeling of plasmas requires innovative numerical algorithms that are tuned to solve the specific physical models that capture the multi-scale and multi-physics phenomena that are present in plasmas.

1.1 Plasma Models: MHD, Kinetic, PIC

Understanding and predictability of plasma behavior has been significantly advanced through the development of reduced plasma models and their numerical solution. The most common reduced plasma model is the magnetohydrodynamic (MHD) model, which describes the plasma as a single-fluid. While the MHD model has been successful in many applications, [1–6] more complex effects require more complete physical models.

The most complete continuum model for plasma is described using kinetic theory where each species α of a plasma is described by a time-dependent distribution function $f_\alpha(\mathbf{x}, \mathbf{v}, t)$ in physical and velocity space. The evolution of the distribution functions is described by the Boltzmann equation

$$\frac{\partial f_\alpha}{\partial t} + \mathbf{v} \cdot \frac{\partial f_\alpha}{\partial \mathbf{x}} + \frac{q_\alpha}{m_\alpha} \left(\mathbf{E} + \mathbf{v} \times \mathbf{B} \right) \cdot \frac{\partial f_\alpha}{\partial \mathbf{v}} = \left. \frac{\partial f_\alpha}{\partial t} \right|_c . \tag{1}$$

The plasma is composed of ion and electron species and possibly additional species for neutrals or impurity ions.

The collision term on the right-hand side of the Boltzmann equation accounts for changes to f_α due to short-range interactions within species α, between species α and species β, and between species β and species γ. The three collisional interactions refer to thermodynamic equilibration within a species, thermodynamic equilibration between species, and species production through atomic reactions, e.g. ionization, recombination, charge exchange. The Boltzmann equation coupled with Maxwell's equations for electromagnetic fields completely describe the plasma dynamics. Plasmas have been simulated using this model with specific forms of the collision operator (e.g. Vlasov equation and Fokker-Planck equation). [7–16] However, the Boltzmann equation spans six dimensions corresponding to spatial position and velocity, in addtion to time. As a consequence of the large dimensionality plasmas are simulated using the Boltzmann equation only when required to capture the essential physics. The applications are generally limited to plasmas with narrow distributions, small spatial extent, and short time durations.

Particle in cell (PIC) plasma models apply the Boltzmann equation to representative superparticles, which are far fewer than the number of particles in the actual plasma. [17] In this manner, PIC methods provide a statistical sampling of phase space. While PIC methods have been successful in modeling many physical effects [18–20], they are not universally applicable due to grid effects and statistical errors or particle noise, which scales with the number of particles as $N^{-1/2}$ [21]. PIC simulations have similar limitations as simulations using kinetic theory.

Another approach to capture more complete physics is to generalize the single-fluid MHD model that results from moments of the Boltzmann equation, Eq. (1). The generalization described here allows for multiple species, and the resulting model is the multi-fluid plasma model. Each fluid is assumed to have a Maxwellian velocity distribution. The generalization also allows for atomic reactions such ionization, recombination, and charge exchange. Furthermore, the moment equations can include higher moments to more accurately model the evolution of plasmas that deviate from thermodynamic equilibrium.

1.2 Introduction to Fluid Plasma Models

Taking moments of the Boltzmann equation, Eq. (1), provides equations that govern the evolution of the moment variables. The moment variables are defined from moments of the distribution function. For example,

$$n_\alpha = \int f_\alpha(\mathbf{v}) d\mathbf{v}, \tag{2}$$

$$n_\alpha u_{\alpha_i} = \int v_i f_\alpha(\mathbf{v}) d\mathbf{v}, \tag{3}$$

$$\vdots$$

where the integrals are performed over all velocity space and i represents the spatial coordinate index. The resulting fluid variables are number density n_α, velocity u_{α_i}, etc. Moments of the Boltzmann equation provide evolution equations for these moment variables. The governing equations for the limiting case of a collisionless plasma with only two species, ions and electrons, the two-fluid plasma model is presented in Ref. [22].

The governing equations of the two-fluid plasma model can be combined to form the single-fluid MHD model. [23] In the derivation of the MHD model several approximations are made, which limit its applicability to low frequency phenomena and ignores potentially significant finite electron mass and charge separation effects. These limitations are not present in the multi-fluid plasma model.

Generalizing the moment approach to include an arbitrary number of species and to include atomic reactions yields the multi-fluid plasma model. The derivation follows that presented, for example, by Braginskii in Ref. [24]. However, the form of the equations are derived here for the conservation variables in flux/source form where

hyperbolic and parabolic fluxes are in balance with source terms. The equation systems can be expressed as

$$\frac{\partial}{\partial t} q_\alpha + \frac{\partial}{\partial x_k} F_{\alpha_k} = S_\alpha, \tag{4}$$

where q_α is the vector of conservation variables of species α, $\mathbf{F}_\alpha$ is the tensor of hyperbolic fluxes for α, and S_α is the source vector for α. Note that throughout this proposal vectors and tensors are represented in bold, and their components are represented in italics with subscript indices (i, j, k, l). Repeated indices of the spatial coordinate are summed in the usual convention of Einstein notation. The source vector includes the coupling to the other fluid species and to the electromagnetic fields. For example, the electric and magnetic fields appear in the source terms of any charged-fluid equations. The field dynamics are governed by Maxwell's equations, which have source terms that contain the charged-fluid variables. See Sec. 1.4. Maxwell's equations can be expressed in the form given by Eq. (4) where $\alpha = EM$.

Since each evolution equation derived from the moment approach introduces the next higher moment, the series continues indefinitely. The equation system must be terminated and closure relations must be specified that relate the higher moment variables to the lower moment variables in the system. The complete multi-fluid model and its extensions are presented in Sec. 1.3.

1.3 The Multi-Fluid Plasma Model

The governing equations for multi-fluid plasma models are derived by taking moments of the Boltzmann equation, Eq. (1), for each species, as briefly introduced in Sec. 1.2. The multi-fluid plasma model (including the electromagnetic equations) are expressed in divergence form as in Eq. (4). Each fluid is assumed to be sufficiently close to thermodynamic equilibrium that its velocity distribution function is well approximated by a limited expansion about a Maxwellian distribution. The fluid variables are derived by taking moments of the distribution function.

$$\rho_\alpha = m_\alpha \int f_\alpha(\mathbf{v}) d\mathbf{v}, \tag{5}$$

$$\rho_\alpha u_{\alpha_i} = m_\alpha \int v_i f_\alpha(\mathbf{v}) d\mathbf{v}, \tag{6}$$

$$p_\alpha = \rho_\alpha T_\alpha = m_\alpha \int \frac{1}{3} \mathbf{w}^2 f_\alpha(\mathbf{w}) d\mathbf{w}, \tag{7}$$

where m_α is the mass of species α, and the distribution function is expressed equivalently as a function of either the velocity $\mathbf{v}$ or the random velocity about the mean fluid velocity $\mathbf{w} = \mathbf{v} - \mathbf{u}_\alpha$. The fluid variables for each species are mass density ρ_α (1 component), velocity $\mathbf{u}_\alpha$ (3 components), and pressure p_α (1 component). T_α is the temperature associated with species α. The model has a total of five fluid variables or components for each species and is called the $5N$-moment fluid model.

An evolution equation for the mass density of each species is given by the zeroth moment of the Boltzmann equation.

$$\frac{\partial}{\partial t}\rho_\alpha + \frac{\partial}{\partial x_k}\left(\rho_\alpha u_{\alpha_k}\right) = \left.\frac{\partial}{\partial t}\rho_\alpha\right|_\Gamma \tag{8}$$

The net mass production rate of species α due to atomic reactions is denoted on the right-hand side of the equation with a subscript Γ. Contributions due to atomic reactions are described later in Sec. 1.4.2.

The first moment of the Boltzmann equation yields momentum equations and describes the evolution of the momentum density for each species.

$$\frac{\partial}{\partial t}\left(\rho_\alpha u_{\alpha_i}\right)+\frac{\partial}{\partial x_k}\left(\rho_\alpha u_{\alpha_i} u_{\alpha_k} + p_\alpha I_{ik}\right) = q_\alpha n_\alpha\left(E_i + \epsilon_{ijk} u_{\alpha_j} B_k\right) - \sum_\beta R_{\alpha\beta_i} + \left.\frac{\partial}{\partial t}\left(\rho_\alpha u_{\alpha_i}\right)\right|_\Gamma \tag{9}$$

where $\mathbf{E}$ and $\mathbf{B}$ are the electric and magnetic fields and $\mathbf{R}_{\alpha\beta}$ is the momentum transfer vector from species α to species β due to collisions. $\mathbf{I}$ is the identity tensor. The number density has been introduced and is defined by $n_\alpha \equiv \rho_\alpha / m_\alpha$. The net momentum production rate of species α due to atomic reactions is denoted on the right-hand side of the equation with a subscript Γ.

The second moment of the Boltzmann equation yields an energy equation for each species, which is expressed in divergence form for the total energy.

$$\frac{\partial}{\partial t}\varepsilon_\alpha + \frac{\partial}{\partial x_k}\left[\left(\varepsilon_\alpha + p_\alpha\right) u_{\alpha_k} + h_{\alpha_k}\right] = q_\alpha n_\alpha u_{\alpha_j} E_j + \sum_\beta u_{\alpha_j} R_{\alpha\beta_j} + \sum_\beta Q_{\alpha\beta} + + \left.\frac{\partial}{\partial t}\varepsilon_\alpha\right|_\Gamma \tag{10}$$

where $\mathbf{h}_\alpha$ is the heat flux vector, $Q_{\alpha\beta}$ is the heat generated in species α due to collisions with species β, and the total energy is defined by

$$\varepsilon_\alpha \equiv \frac{1}{\gamma - 1} p_\alpha + \frac{1}{2}\rho_\alpha u_{\alpha_j}^2 \tag{11}$$

and γ is the ratio of specific heats. The evolution equation for the total energy can be combined with the previous two moment equations to provide an expression for the evolution of pressure. The energy addition rate of species α due to atomic reactions is denoted on the right-hand side of the equation with a subscript Γ.

Since the heat flux represents a higher moment of the distribution function, a closure relation must be specified that relates it to the lower moment variables. Fourier's law is a commonly used relation, which gives the i^{th} component of the heat flux as

$$h_{\alpha_i} = -\kappa_{\alpha_{ij}} \frac{\partial}{\partial x_j} T_\alpha, \tag{12}$$

where $\kappa_{\alpha_{ij}}$ is the ij component of the thermal conductivity tensor which, in general, depends on the strength and relative orientation of the magnetic field. Additional

closure relations are needed if a pressure tensor is used instead of the scalar pressure used in the momentum and energy evolution equations.

The $5N$-moment model and appropriate closures are derived using a Chapman-Enskog expansion of the distribution function. The distribution function is assumed to be a Maxwellian (thermodynamic equilibrium) distribution with an expansion in powers of a small parameter given by the Knudsen number, the ratio of the mean free path to the characteristic plasma size. Closure relations for the transport coefficients are found by retaining only the linear terms of the expansion. For examples of calculations of transport coefficients, see Ref. [24, 25].

1.4 Maxwell's Equations

The electromagnetic fields influence the motion of the plasma fluid through the Lorentz force, which is contained in Eq. (1) for the kinetic model, Eq. (9) for the $5N$-moment model, and Eq. (43) for the $13N$-moment model. The motion of the plasma influences the evolution of the electromagnetic fields through the redistribution of charge density and current density. Maxwell's equations govern the evolution of the electromagnetic fields. The net charge density and total current density are calculated directly from the plasma state, i.e. the distribution functions or the multi-fluid plasma variables, as

$$\rho_c = \sum_\alpha q_\alpha n_\alpha = \sum_\alpha q_\alpha \int f_\alpha(\mathbf{v}) d\mathbf{v} \tag{13}$$

$$j_i = \sum_\alpha q_\alpha n_\alpha u_{\alpha_i} = \sum_\alpha q_\alpha \int v_i f_\alpha(\mathbf{v}) d\mathbf{v}. \tag{14}$$

These terms appear as source terms in Maxwell's equations, which can be expressed as

$$\frac{\partial}{\partial t} B_i = -\epsilon_{ijk} \frac{\partial}{\partial x_j} E_k \tag{15}$$

$$\epsilon_0 \mu_0 \frac{\partial}{\partial t} E_i = \epsilon_{ijk} \frac{\partial}{\partial x_j} B_k - \mu_0 j_i \tag{16}$$

$$\epsilon_0 \frac{\partial}{\partial x_k} E_k = \rho_c \tag{17}$$

$$\frac{\partial}{\partial x_k} B_k = 0 \tag{18}$$

The divergence constraint relations on $\mathbf{E}$ and $\mathbf{B}$ should not enter the calculation of the field dynamics. Mathematically, if the initial fields satisfy the divergence constraints, then the field evolution maintains the constraints. Numerically, the divergence constraints must be explicitly enforced by "cleaning" the fields with either an elliptic method [26], a hyperbolic method [27], or a parabolic method [28].

The Jacobians of the hyperbolic fluxes $\partial \mathbf{F}_\alpha / \partial q_\alpha$ of the governing equations are constructed in the usual way from Eq. (4). The eigenvalues of the flux Jacobians give

the characteristic velocities. In one dimension, the eigenvalues of the fluid equations are

$$\lambda_{fluid} = \{v_{\alpha_x}, v_{\alpha_x} \pm c_{s_\alpha}\} \tag{19}$$

where the acoustic speed for species α is defined as

$$c_{s_\alpha} = \sqrt{\frac{\gamma T_\alpha}{m_\alpha}}. \tag{20}$$

The electron acoustic speed is larger than the ion acoustic speed for the same fluid temperatures due to the large ion to electron mass ratio. The electron acoustic speed can be larger than the Alfvén speed, which is a component of the eigenvalues of MHD. The Alfvén speed for an ion/electron plasma is defined as

$$v_A = \frac{B}{\sqrt{\mu_0 \left(m_i n_i + m_e n_e\right)}} \tag{21}$$

where B is the magnitude of the magnetic field and μ_0 is the permeability of free space ($4\pi \times 10^{-7}$ H/m). The eigenvalues of the field equations are

$$\lambda_{field} = \{\pm c\}, \tag{22}$$

where c is the speed of light. Therefore, the eigenvalues of the multi-fluid plasma model are generally not bounded by the eigenvalues of the MHD model. In general, the fastest times that must be resolved in the multi-fluid plasma model are the timescales associated with the electromagnetic fields and the electron fluid, namely, the light transit time and the electron plasma oscillation period.

1.4.1 Collisional Effects

The fluids of the multi-fluid plasma model interact primarily through the electromagnetic fields, which produce long-range forces. However, short-range collisional effects can have a significant impact on the overall plasma behavior and evolution. Specifically, collisional effects can thermalize the fluids such that the entire plasma approaches a thermodynamic equilibrium. The time for thermalization within a species is the self-relaxation time. Collisions between species bring the fluids into thermodynamic equilibration with a characteristic relaxation time. For example, an electron-ion fluid plasma typically has relaxation times such that $\tau_{ee} \ll \tau_{ii} \ll \tau_{ie}$.

Collisional effects are formally treated in the fluid model by evaluating the collision integral, the right-hand side of Boltzmann equation, Eq. (1). The Landau form of the collision integral for Coulomb collisions [29] is expressed as

$$\begin{aligned}\left.\frac{\partial f_\alpha}{\partial t}\right|_c &= \sum_\beta C_{\alpha\beta} \\ &= \sum_\beta \frac{2\pi}{m_\alpha}\left(\frac{q_\alpha q_\beta}{4\pi\epsilon_0}\right)^2 \ln\Lambda \frac{\partial}{\partial v_k}\int U_{kl}\left(\frac{f_\beta(\mathbf{v}')}{m_\alpha}\frac{\partial}{\partial v_l} f_\alpha(\mathbf{v}) - \frac{f_\alpha(\mathbf{v})}{m_\beta}\frac{\partial}{\partial v_l'} f_\beta(\mathbf{v}')\right) d\mathbf{v}',\end{aligned} \tag{23}$$

where

$$U_{kl} = \frac{1}{\left(v_j - v_j'\right)^3}\left[\left(v_j - v_j'\right)^2 \delta_{kl} - \left(v_k - v_k'\right)\left(v_l - v_l'\right)\right]. \tag{24}$$

The collisional terms accounts for transfer of momentum and energy between the different fluids. [24] The terms appear as frictional effects in Eqs. (9) and (10), $\sum_\beta R_{\alpha\beta_i}$. In general, the momentum transfer vector is defined by the first moment of the collision integral with the random velocity, as used in Eq.(7),

$$R_{\alpha\beta_i} = m_\alpha \int w_i C_{\alpha\beta} d\mathbf{w}. \tag{25}$$

If only binary collisions that result in small angle deflections are included, the rate of momentum transfer from species α to species β is given by

$$R_{\alpha\beta_i} = \frac{m_\beta}{m_\alpha + m_\beta}\rho_\alpha \nu_{\alpha\beta}\left(v_{\alpha_i} - v_{\beta_i}\right), \tag{26}$$

where $\nu_{\alpha\beta}$ is the collision frequency between species α and β. Momentum conservation requires $R_{\alpha\beta_i} = -R_{\beta\alpha_i}$ and $R_{\alpha\alpha_i} = 0$. Heat generation due to random collisions is defined by the second moment of the collision integral with the random velocity,

$$Q_{\alpha\beta} = \frac{1}{2} m_\alpha \int \mathbf{w}^2 C_{\alpha\beta} d\mathbf{w}. \tag{27}$$

These relations hold for nonreacting collisions, such as elastic collisions. Including atomic reactions requires a generalization or additional effects to the collisional effects. Including the effect of atomic reactions on the plasma dynamics requires additional terms in the collision operator, and is described in the next section.

1.4.2 Atomic Reactions

The purpose of including the effect of atomic reactions into the multi-fluid plasma model is to capture the time-dependent ionization, recombination, and charge exchange reactions that are important in laboratory and transient plasmas. Atomic reactions lead to the transfer of density, momentum, and energy between the fluids in the multi-fluid plasma model. For example, ionization depletes the neutral fluid and increases the ion and electron fluids.

Contributions from atomic reactions are identified by terms on the right-hand side of Eqs. (8), (9), and (10). The terms are expressed below for the ionization (ion), recombination (rec), and charge exchange (cx) reactions for a hydrogen plasma composed of neutral hydrogen ($\alpha = n$), ionized hydrogen ($\alpha = i$), and electrons ($\alpha = e$). Additional reactions and other plasma constituents are also possible.

The formal procedure to account for atomic reactions in the fluid model requires evaluating the collision integral, the right-hand side of Boltzmann equation. The evaluation involves convolving the distribution functions of the reacting species with the

reaction cross section that depends on their relative velocities. For example, the resulting effect on the ion species from charge exchange reactions with the neutral species is

$$\left.\frac{\partial f_i}{\partial t}\right|_c = \int \sigma_{cx} \left|\mathbf{v}' - \mathbf{v}\right| \left[f_i(\mathbf{v}') f_n(\mathbf{v}) - f_i(\mathbf{v}) f_n(\mathbf{v}')\right] d\mathbf{v}', \tag{28}$$

where $\sigma_{cx} = \sigma_{cx}\left(|\mathbf{v}' - \mathbf{v}|\right)$ is the cross section for charge exchange. [30]

Evaluating Eq. (28) is accomplished by assuming distribution functions for each species, for example a Chapman-Enskog expansion. Zeroth order contributions are found by assuming a Maxwellian distribution. These are presented below. More detailed calculations will be performed for the proposed work to include higher order corrections that account for small deviations away from Maxwellian.

The contributions to the species densities are

$$\left.\frac{\partial}{\partial t}\rho_n\right|_\Gamma = m_n\left(-\Gamma_{ion} + \Gamma_{rec}\right), \tag{29}$$

$$\left.\frac{\partial}{\partial t}\rho_i\right|_\Gamma = m_i\left(\Gamma_{ion} - \Gamma_{rec}\right), \tag{30}$$

$$\left.\frac{\partial}{\partial t}\rho_e\right|_\Gamma = m_e\left(\Gamma_{ion} - \Gamma_{rec}\right). \tag{31}$$

The contributions to the species momenta are

$$\left.\frac{\partial}{\partial t}\left(\rho_n u_{n_i}\right)\right|_\Gamma = -\left(\Gamma_{ion} + \Gamma_{cx}\right) m_n u_{n_i} + \left(\Gamma_{rec} + \Gamma_{cx}\right) m_i u_{i_i}, \tag{32}$$

$$\left.\frac{\partial}{\partial t}\left(\rho_i u_{i_i}\right)\right|_\Gamma = \left(\Gamma_{ion} + \Gamma_{cx}\right) m_i u_{n_i} - \left(\Gamma_{rec} + \Gamma_{cx}\right) m_i u_{i_i}, \tag{33}$$

$$\left.\frac{\partial}{\partial t}\left(\rho_e u_{e_i}\right)\right|_\Gamma = \left(\Gamma_{ion} + \Gamma_{cx}\right) m_e u_{n_i} - \left(\Gamma_{rec} + \Gamma_{cx}\right) m_e u_{e_i}. \tag{34}$$

The contributions to the species energies are

$$\left.\frac{\partial}{\partial t}\varepsilon_n\right|_\Gamma = -\left(\Gamma_{ion} + \Gamma_{cx}\right)\varepsilon_n + \left(\Gamma_{rec} + \Gamma_{cx}\right)\varepsilon_i, \tag{35}$$

$$\left.\frac{\partial}{\partial t}\varepsilon_i\right|_\Gamma = \left(\Gamma_{ion} + \Gamma_{cx}\right)\varepsilon_n - \left(\Gamma_{rec} + \Gamma_{cx}\right)\varepsilon_i, \tag{36}$$

$$\left.\frac{\partial}{\partial t}\varepsilon_e\right|_\Gamma = \left(\Gamma_{ion} + \Gamma_{cx}\right)\varepsilon_n - \left(\Gamma_{rec} + \Gamma_{cx}\right)\varepsilon_e. \tag{37}$$

The reaction rates are given by

$$\begin{aligned} \Gamma_{ion} &= \langle\sigma v\rangle_{ion} n_n n_i \\ \Gamma_{rec} &= \langle\sigma v\rangle_{rec} n_e n_i \\ \Gamma_{cx} &= \langle\sigma v\rangle_{cx} n_n n_i \end{aligned} \tag{38}$$

As indicated in Eq. (28), the cross sections σ and reaction rate parameters $\langle\sigma v\rangle$ can depend on temperature.

1.5 Higher Moment Models

The $5N$-moment model presented above provides an adequate description for many plasmas that have relaxed sufficiently close to thermodynamic equilibrium. For truly non-equilibrium plasmas, a kinetic model is needed. Generalizations of the moment method (higher moment models) extend the applicability of fluid models to non-equilibrium plasmas. The higher moments extend the ability to characterize the distribution function with averaged or moment variables.

The $13N$-moment model provides the next logical extension of the $5N$-moment plasma model. The model as first introduced by Grad [31] and has since been refined by many others, for example Refs. [32–36]. Specifically, Ref. [32] provides a derivation for gas dynamics using a Pearson-type-IV distribution for the velocity distribution function that better matches experimental measurements and improves the hyperbolicity of the resulting evolution equations. These are important advantages over Grad's initial method. The results are only briefly presented here for a neutral gas. We have extend the model to derive a $13N$-moment fluid model for a multicomponent plasma.

As before, moments of the distribution function provide the fundamental fluid variables. Consistent with the original derivation by Grad [31], only the variables with an explicit physical meaning are retained. For each species fluid the density and velocity is defined as in Eqs. (5) and (6). The scalar pressure is replaced with the pressure tensor and the heat flux vector is also defined as a solution variable. These variables are defined as

$$p_{ij} = m \int w_i w_j f(\mathbf{w}) d\mathbf{w}, \tag{39}$$

$$h_i = m \int \frac{1}{2} \mathbf{w}^2 w_i f(\mathbf{w}) d\mathbf{w}, \tag{40}$$

where the species subscript α has been dropped for clarity. In addition to the 4 components of density and velocity, the model has a total of thirteen fluid variables or components for each fluid. The pressure tensor $\mathbf{p}$ has 6 components, since $p_{ij} = p_{ji}$ and heat flux $\mathbf{h}$ has 3 components. Note the scalar pressure is the trace of the pressure tensor, and is given by

$$p = \rho T = m \int \frac{1}{3} \mathbf{w}^2 f(\mathbf{w}) d\mathbf{w}, \tag{41}$$

which is consistent with the definition from Eq. (7).

Taking moments of the Boltzmann equation provides the evolution equations for the moment variables.

$$\frac{\partial}{\partial t} \rho + \frac{\partial}{\partial x_k} \left(\rho u_k \right) = 0, \tag{42}$$

$$\frac{\partial}{\partial t} \left(\rho u_i \right) + \frac{\partial}{\partial x_k} \left(\rho u_i u_k + p_{ik} \right) = 0, \tag{43}$$

$$\frac{\partial}{\partial t} \left(\rho u_i u_j + p_{ij} \right) + \frac{\partial}{\partial x_k} \left(\rho u_i u_j u_k + 3 p_{ij} u_k + m_{ijk} \right) = 0, \tag{44}$$

$$\frac{\partial}{\partial t}\left[\frac{\rho u_j^2 + p_{jj}}{2}u_i + p_{ij}u_j + h_i\right] + \frac{\partial}{\partial x_k}\left[\frac{\rho u_j^2 + p_{jj}}{2}u_i u_k + \frac{p_{ik}u_j^2}{2} + 2u_i p_{jk}u_j + 2h_i u_k + m_{ijk}u_j + \frac{R_{ik}}{2}\right] = 0. \quad (45)$$

Equations (44) and (45) provide evolution equations for the pressure tensor and heat flux vector. The equation system must be closed for the variables corresponding to the higher moments, namely,

$$m_{ijk} = m\int w_i w_j w_k f(\mathbf{w}) d\mathbf{w}, \quad (46)$$

$$R_{ij} = m\int \mathbf{w}^2 w_i w_j f(\mathbf{w}) d\mathbf{w}. \quad (47)$$

Closure relations are derived by assuming a particular form of the distribution function. For the proposed work, a Pearson-type-IV distribution will be used, as in Ref. [32].

1.6 Computational Solution Methods

The computational methods used to solve the multi-fluid plasma model and Maxwell's equations described above are developed to be optimally matched for the expected physics for each set of governing equations. The spatial representation for all of the system variables is based on finite element methods where the simulation domain is divided into discrete elements, which are either quadrilaterals (2D) or hexahedrals (3D). The variation of the solution variables within each element are modeled by projecting the variables onto a set of spatially dependent basis functions v_h of order h, such that within each element Ω variable q is represented as

$$q_\Omega(\mathbf{x}) = \sum_h q_{\Omega_h} v_h(\mathbf{x}). \quad (48)$$

The basis functions are Legendre polynomials or Jacobi polynomials for the proposed implementation. The finite element representation captures high-order spatial variations, which is critical when anisotropic properties exist [37] or when hyperbolic fluxes are balanced by the fluxes from other species, which occurs at equilibrium.

The governing equations for the multi-fluid plasma model can be expressed as given by Eq. (4). The equations can be grouped according to their physically characteristic spatial and temporal scales, which forms the basis for selecting the appropriate computational method. The fast temporal and short spatial dynamics of the electron fluid and electromagnetic fields suggests solving these governing equations in a coupled manner as

$$\frac{\partial}{\partial t}\begin{bmatrix} q_{EM} \\ q_e \end{bmatrix} + \frac{\partial}{\partial x_k}\begin{bmatrix} F_{EM_k} \\ F_{e_k} \end{bmatrix} = \begin{bmatrix} S_{EM} \\ S_e \end{bmatrix}, \quad (49)$$

where the source terms, in general, depend on the solution variables of the fields and other species, $S_\alpha = S_\alpha\left(q_{EM}, q_e, q_i, q_n\right)$. The slow temporal and long spatial dynamics of the ion and neutral fluids suggests solving these governing equations in a separately coupled manner as

$$\frac{\partial}{\partial t}\begin{bmatrix} q_i \\ q_n \end{bmatrix} + \frac{\partial}{\partial x_k}\begin{bmatrix} F_{i_k} \\ F_{n_k} \end{bmatrix} = \begin{bmatrix} S_i \\ S_n \end{bmatrix}, \tag{50}$$

where the source terms again, in general, depend on the solution variables of the fields and other species.

A Galerkin method is used to obtain spatially discretized equations. The governing equations are multiplied by each basis function and integrated over the element volume to give the integral equation

$$\int_\Omega v_h \frac{\partial q}{\partial t} dV + \oint_{\partial\Omega} v_h F_k dA_k - \int_\Omega F_k \frac{\partial}{\partial x_k} v_h dV = \int_\Omega v_h S dV. \tag{51}$$

The integrals are evaluated by Gaussian quadrature. The source terms are also projected onto the basis functions, similar to Eq. (48). The solution of Eq. (51) throughout the spatial domain and its time advance provides the complete time-dependent solution. Both the spatial representation and time advance are optimized based on the expected physics.

1.7 Implementation and Computational Demonstrations

This section provides a brief description of the implementation details and presents demonstrations of the computational algorithm generated by our Computational Plasma Dynamics Group at the University of Washington. We have developed accurate numerical algorithms for the two-fluid plasma model that are based on finite volume [22, 38] and DG methods [39–42]. Higher moment plasma models ($10N$ and $13N$) have been derived and investigated. [34–36, 43] Numerical formulations have been investigated that allow for the implicit solutions of plasma models. [2] These computational advances have been applied to study plasma phenomena with high fidelity models, e.g. Refs. [44–46]. In addition, we have developed non-reflecting open boundary conditions that allow simulating infinite space on finite domains. [47, 48] The results described here focus on our developments of the FE method that we have applied to continuum plasma models and on our implementation of appropriate boundary conditions. The algorithm research and development have been implemented in a flexible software framework called WARPX (Washington Approximate Riemann Plasma), which uses C++ object oriented programming and other modern software techniques to simplify the maintainability and extensibility of the code and HDF5 for parallel output. WARPX uses MPI message passing for parallel computer architectures and OpenCL for GPU/many-core computer architectures.

1.7.1 Multi-Fluid Plasma Model

We have developed a DG method [49–51] to solve the governing equations of the multi-fluid plasma model on a computational grid. The DG method is a finite element approach that allows for arbitrarily high-order basis functions to model the variation of the system variables, as described in Sec. 1.6 and in more detail in the references provided.

The surface integral in Eq. (51) uses numerical hyperbolic fluxes computed with a Roe-type approximate Riemann solver [22, 39, 52] or with a Lax-Friedrich flux [40]. The overall solution is built upon the solutions to the Riemann problem defined by the discontinuous jumps in the solution at each element interface. Continuity of the fluxes between the elements ensures conservation. The numerical flux for a first-order accurate (in space) Roe-type solver is written in symmetric form as

$$F_{i+1/2} = \frac{1}{2}\left(F_{i+1} + F_i\right) - \frac{1}{2}\sum_k l_k \left(q_{i+1} - q_i\right) |\lambda_k| \, r_k \tag{52}$$

where r_k is the k^{th} right eigenvector, λ_k is the k^{th} eigenvalue, and l_k is the k^{th} left eigenvector, evaluated at the element interface $(i + 1/2)$. The values at the element interface are obtained by a Roe average of the neighboring elements. The flux calculated as above is normal to the element interface which is the desired orientation for calculating the surface integral.

As a simple example, a the two-dimensional, second-order accurate algorithm, uses a set of linear basis functions.

$$\{v_h\} = \{v_0, v_x, v_y\} = \left\{1, \frac{x - x_{ij}}{\Delta x/2}, \frac{y - y_{ij}}{\Delta y/2}\right\} \tag{53}$$

where the center of the mesh element is located at (x_{ij}, y_{ij}) and extends Δx by Δy. The conserved variables q are defined as

$$q = q_0 + q_x v_x + q_y v_y \tag{54}$$

within each mesh element. The DG method has been implemented using a modal approach, as opposed to the nodal approach that is common in typical FE methods. Update equations for the coefficients for each conserved variable are found directly from Eq. (51) applied to each mesh element. The temporal evolution is computed with a Runge-Kutta method. A third order TVD method has been used successfully. [53]

High-order FE methods more accurately capture fine scale structures, which is demonstrated by studying the propagation of dispersive waves. Electrostatic ion cyclotron waves produce dispersive waves which have an analytical description. A wave with frequency ω and wave number k is described by the dispersion relation, $\omega^2 = k^2 c_s^2 + \omega_c^2$, where c_s is the sound speed and ω_c is the cyclotron frequency. Nine modes are excited, such that the analytic solution evolves to contain many frequencies and wave numbers, as seen in Fig. 1. We simulated the problem using the DG method

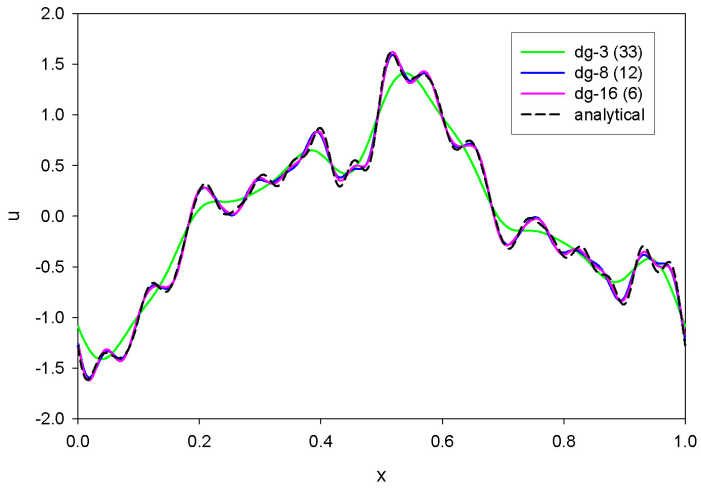

Figure 1: Dispersive electrostatic ion cyclotron waves generated from a nine mode excitation. Plotted is the analytical solution and numerical solutions with a fixed number of unknowns: 3rd order DG with 33 elements (dg-3), 8th order DG with 12 elements (dg-8), and 16th order DG with 6 elements (dg-16). The benefit of high-order is evident.

with different orders of accuracy but with the same effective resolution (approximately constant number of unknowns). [42] The results in Fig. 1 show that a high-order DG method better matches the analytical solution.

High-order FE methods also better resolve anisotropic behavior that often results in magnetized plasmas. The ratio of parallel to perpendicular thermal conductivities can be as large as 10^6. Low-order methods introduce significant numerical diffusion that obscures the anisotropic transport properties. We have investigated the ability of high-order FE to resolve perfect heat conduction along a toroidal magnetic field in a Cartesian grid, where the ratio of the conductivities is $D_\perp/D_\parallel = 0$. [37] The results are presented in Fig. 2, which show that higher-order FE maintains a lower numerically measured $D_\perp$ even for the same effective resolution.

The discontinuous Galerkin algorithm has been applied to the electromagnetic plasma shock demonstrating the transition from gas dynamic shocks to the MHD shock [54, 55] as the Larmor radius is reduced. Analysis of the data shows the differences caused by the additional plasma waves that are captured in the two-fluid model and, consequently. [22] It also illustrates the dispersive nature of the waves, which makes capturing the effect difficult in MHD algorithms. The electromagnetic plasma shock serves to validate the algorithm to published data (MHD limit) and analytical results (gas dynamic limit). The algorithm has also been applied to study collisionless reconnection and the results are compared to published results of the GEM challenge problem. [56] The problem is difficult to model and provides a rigorous test for the algorithm and benchmarks to other algorithms. The evolution of the reconnected magnetic

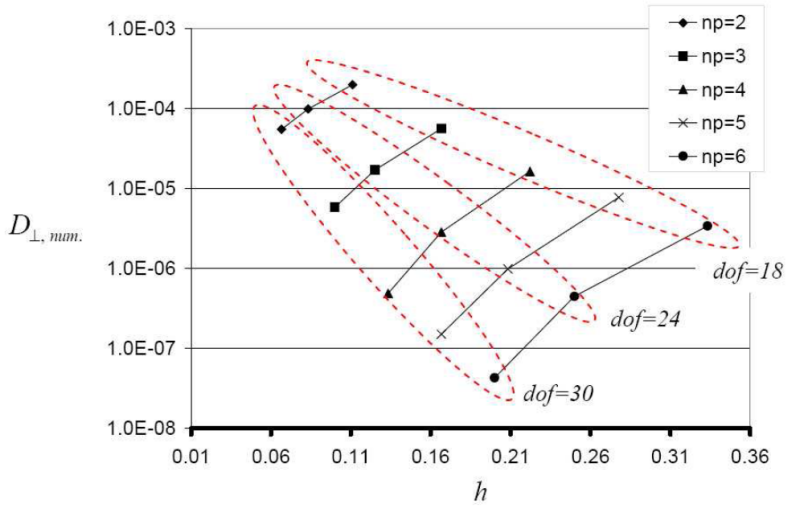

Figure 2: Numerically measured thermal conductivity perpendicular to a toroidal magnetic field. Analytically, $D_\perp$ should be zero. Plotted are the values of $D_\perp$ for different element size (h) and FE order (np). Higher-order FE maintains a lower $D_\perp$ even for the same effective resolution (dof). The benefit of high-order is evident.

flux compares remarkably well with the published data. [39]

Additional applications of the $5N$-moment plasma fluid model have investigated lower hybrid drift instabilities to explain anomalous resistivity observed in experimental plasmas [45] and the evolution of FRC plasmas [44]. Applications have also isolated and contrasted the physics captured by the multi-fluid plasma model and Hall-MHD model. [46]

We have also developed advanced physics models that describe plasma-neutral interactions in a computationally tractable manner. [57] The addition of a neutral fluid has enabled modeling of plasma interactions with neutral flows and sheath formations. [41, 58] These simulations have demonstrated the generation of a nonlinear Langmuir wave that propagates away from the electrodes.

The $13N$-moment plasma fluid model represents a unique advance because it extends the region of validity of moment models towards the kinetic regime. In this manner, it provides a meaningful step towards bridging the gap. We have developed forms on the $13N$-moment plasma fluid model based on the Pearson-type-IV distribution for the velocity distribution function. Our initial results in Fig. 3 illustrate the relationship between the $5N$-moment model, the $13N$-moment model, and the ∞N-moment model (continuum kinetic model). The kinetic solution is the numerical solution of the Boltzmann equation with a BGK collision operator. A similar collision operator is required for the $13N$-moment model to better approximate the physical processes.

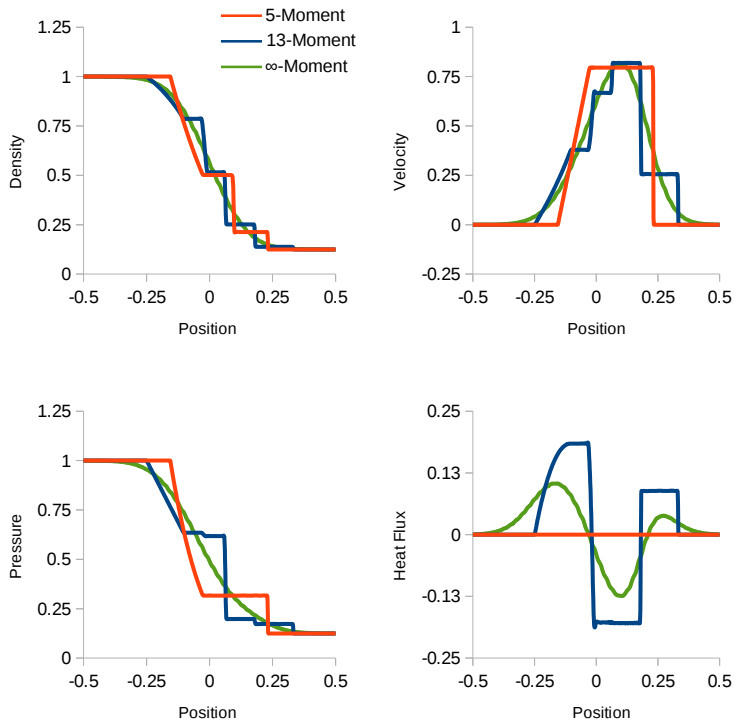

Figure 3: Shock tube simulation with three different plasma models: $5N$-moment model, $13N$-moment model, and ∞N-moment model (continuum kinetic model). The comparison illustrates the convergence and relationships between the models.

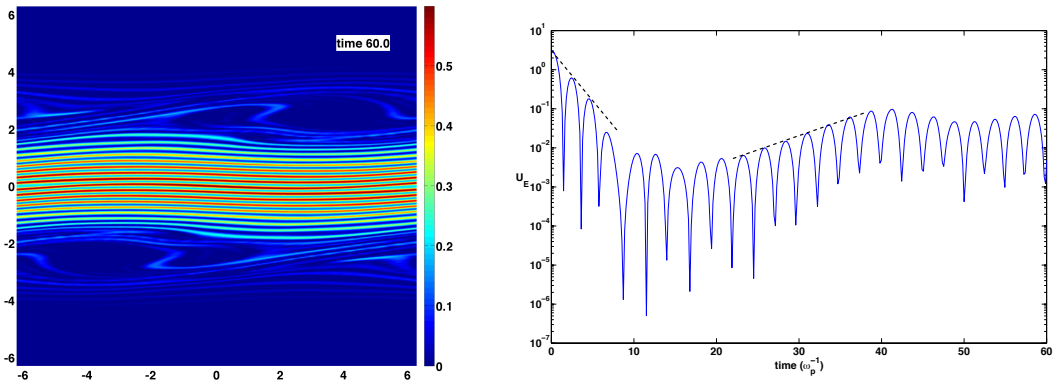

Figure 4: Nonlinear solution of the Vlasov-Poisson equation system for the strong Landau damping problem using seventh-order polynomials on a 20×80 phase-space grid in (x,v_x) at $t = 60\omega_p^{-1}$. Evolution of the potential energy exhibits the expected damping and growth behavior.

1.7.2 Continuum Kinetic Plasma Model

As indicated by the ∞-Moment solution in Fig. 3, we have made substantial progress in solving continuum kinetic plasma models - directly evolving Boltzmann equation, Eq. (1). Using the DG method to solve the Vlasov-Poisson system has recently gained substantial interest. [59, 60] We have also implemented the DG method to solve the Vlasov-Poisson equation system in WARPX. Figure 4 shows the nonlinear solution for the strong Landau damping problem using seventh-order polynomials. The potential energy exhibits the expected damping and growth behavior, and agrees with previously published results. [59, 61] These are preliminary calculations, but they illustrate the broader applicability of the DG method. In particular, high-order representation is able to accurately capture the striations that occur in phase space. We have investigated the conservation properties of our DG method implementation, and mass, momentum, and energy are conserved significantly better than in other continuum implementations.

In addition, we have also developed benchmark problems for continuum kinetic modeling. While several benchmark problems exist, they are limited to electrostatic and two dimensions. [59, 61] We have developed a three dimensional benchmark for magnetized plasmas. [62] It has been initially implemented using a high-order, finite-volume method, but it will also be used for our DG implementation.

1.7.3 Implicit Time Advance and the Blended Finite Element Method

As described in Secs. 1.6 and 1.7.1, both CG and DG finite element methods have been successfully used to solve continuum plasma models. The numerical solution of the governing equations has produced some unique and difficult challenges. Specifically,

the advanced plasma models encompass a wide disparity of spatial and temporal scales that are fundamentally generated by the massive ions and neutrals, lighter electrons, and massless electromagnetic fields. Solving the multi-fluid model requires a numerical algorithm that can capture these multiple scales efficiently and accurately.

Building on the success of the explicit time advance methods, it is logical to investigate implicit time advance methods to alleviate the time-step limitations. Implicit methods allow for time steps that are not limited by the fast waves. The entire system of governing equations, Eq. (4), is rewritten as

$$\frac{\partial}{\partial t}\begin{bmatrix} q_{EM} \\ q_e \\ q_i \\ \vdots \end{bmatrix} = f\left(\begin{bmatrix} q_{EM} \\ q_e \\ q_i \\ \vdots \end{bmatrix}\right), \tag{55}$$

for the electromagnetic fields, electron fluid, and ion fluid, where the right hand side of Eq. (55) includes the hyperbolic fluxes and sources. The time advance can be expressed in an implicit form of arbitrary order accuracy. A second-order Crank-Nicolson method has been implemented, where the time advance equation is written as

$$q^{n+1} = q^n + \frac{\Delta t}{2}\left[f(q^{n+1}) + f(q^n)\right], \tag{56}$$

which is solved iteratively using a variety of implicit numerical methods.

The $5N$-moment multi-fluid plasma model contains 18 variables for the ion and electron fluids and the electromagnetic fields. Each additional fluid requires an additional 5 variables. Formulating an implicit time-advance method results in a large, stiff equation system with a matrix that is difficult to invert. We tested a variety of implicit numerical methods, e.g. Conjugate Residual, Biconjugate Gradient, and GMRES with preconditioners such as Incomplete LU and Additive Schwarz. None have performed adequately without artificially altering the physics of the problem with either unrealistically massive electrons, e.g. $m_i/m_e = 25$, or unphysically slow light speed, e.g. $c/v_A = 10$. The difficulty stems from the widely different masses of the ions and neutrals compared to the electrons and fields. For example, adequately resolving the electrons in space and time results in greatly "over-resolving" the ions and leads to numerical dissipation of the ion features.

This motivated our physics-based computational algorithm, which has been tremendously successful. The algorithm performs a physics-based splitting of the governing equations and applies appropriate spatial and temporal representations the split system while still providing the necessary coupling.

Because of the light mass and high mobility of electrons, electron characteristic speeds (eigenvalues) are fast compared to ions and neutrals. Electrons only form true shocks in extremely rare situations, for example, when the electron or ion flow velocities exceed the electron thermal speed, which does not usually occur since the ions generally move slower than electrons and the ions slow the electron motion. Ions and

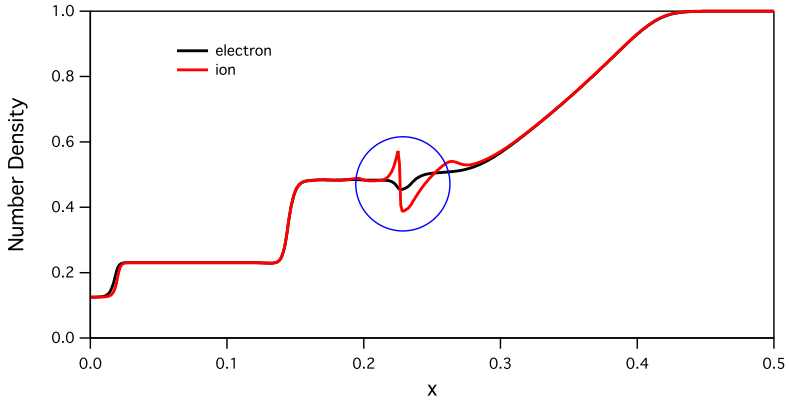

Figure 5: Plasma shock simulation using the two-fluid plasma model with physical values for m_e, m_i, and c. The slow compound wave structure (in blue circle), which is composed of a shock and rarefaction wave, produces a shock in the ion fluid but not the electron fluid. Normalized number density is plotted as a function of position.

neutrals have much slower characteristic speeds, and they can and do form shocks. The electromagnetic coupling between the ions and electrons generates forces that modify the electron spatial structure to approximate the ion spatial structure. If the ions form a shock, the electron spatial structure has a variation, but typically the variation is not a true discontinuity. An example of this behavior is shown in Fig. 5, which shows a plasma shock simulation using the two-fluid plasma model. A "slow compound" (SC) wave structure ($x = 0.23$) has formed at the base of the rarefaction. The SC wave structure is composed of a shock and rarefaction wave. The SC structure produces a shock in the ion fluid, but the electron fluid has only a smooth variation. Since the electromagnetic fields have the fastest characteristic speeds of the system, the fields in the multi-fluid plasma model should never form shocks.

We have developed a blended finite element (BFE) method that applies a high-order, continuous spatial representation (CG method) for the electron fluid and electromagnetic fields and a high-order, discontinuous spatial representation (DG method) for the ion and neutral fluids. The electron fluid and electromagnetic fields do not require inter-element flux calculations or limiting since their solutions are expected to be smooth and well-resolved. The ion and neutral fluids use approximate Riemann fluxes and limiting to capture shocks. Time advance of the electron fluid and electromagnetic fields can be solved implicitly so that their dynamics do not limit the time step. Since the dynamics of the ion and neutral fluids typically set the timescale of interest, their evolution is solved explicitly using the TVD Runge-Kutta method mentioned in Sec. 1.6.

The performance of the BFE method is demonstrated by applying it to study laser-

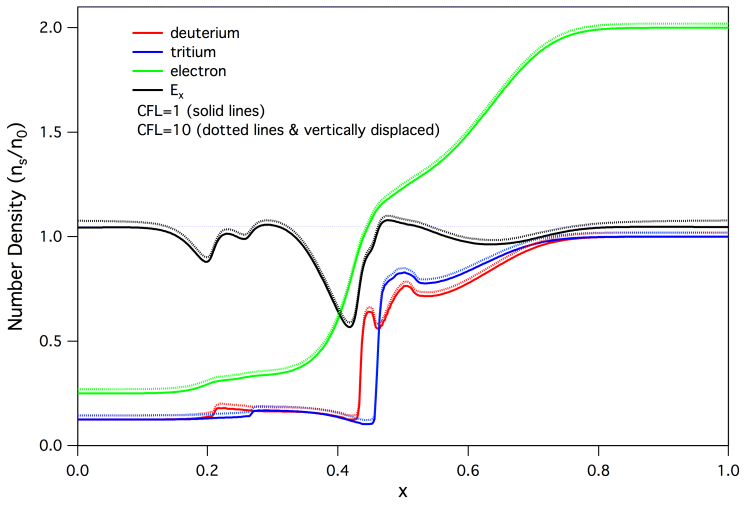

Figure 6: Blended finite element method applied to the species separation problem in capsule implosions. Number densities and electric field are shown after the laser drive has compressed the multi-fluid plasma and caused a species separation. Excellent agreement is found between the explicit and implicit solutions, CFL=1 (solid lines) and CFL=10 (dotted lines displaced vertically for clarity).

driven implosions to compress deuterium-tritium fuel to fusion conditions. Separation of the deuterium and tritium species could explain the experimentally observed low fusion yield. The simulation is performed using the BFE method with the multi-fluid $5N$-moment plasma model for three fluids (deuterium, tritium, and electron). The number densities are shown in Fig. 6 after the laser drive has started the compression. A separation clearly develops. The solution is found using an explicit advance (CFL=1) for the entire solution, q_{EM}, q_e, q_D, q_T. The solution is also found using an implicit advance (CFL=10) for the electron fluid and electromagnetic fields, q_{EM}, q_e, and an explicit advance for the ionic species, q_D, q_T. The agreement can be seen in Fig. 6.

1.7.4 Divergence Cleaning in Maxwell's Equations

Section 1.4 presented Maxwell's equations. The time-dependent equations, Eqs. (15) & (16), completely describe the evolution of the electromagnetic fields. Provided the divergence equations, Eqs. (17) & (18), are initially satisfied, the evolved fields will always satisfy them analytically. However, computational solutions can lead to violations of the divergence constraints (involutions) and corresponding nonphysical effects such as charge generation and parallel magnetic forces.

We have previously investigated several methods to "clean" the divergence errors. These methods have included solving the mixed potential formulation of Maxwell's equations and modifying Maxwell's equations to be purely hyperbolic [27]. Recently, we have investigated a parabolic modification [28] that produces significantly improved results without the computational expense of a mixed potential formulation.

In this approach, the divergence constraint relations are incorporated with the time-dependent field equations as parabolic terms. Faraday's law is transformed by adding a diffusive term proportional to the divergence error, which is written in vector form as

$$\frac{\partial \mathbf{B}}{\partial t} = -\nabla \times \mathbf{E} + \chi_B \nabla \left(\nabla \cdot \mathbf{B} \right) \tag{57}$$

where χ_B is a constant magnetic field divergence error diffusivity. The evolution of the divergence error of the magnetic field is found by taking the divergence of Eq. (57) to give

$$\frac{\partial}{\partial t} \left(\nabla \cdot \mathbf{B} \right) = \chi_B \nabla^2 \left(\nabla \cdot \mathbf{B} \right), \tag{58}$$

which locally diffuses the divergence error. A similar modification of Ampere's law is performed to give

$$\epsilon_0 \mu_0 \frac{\partial \mathbf{E}}{\partial t} = \nabla \times \mathbf{B} - \mu_0 \sum_\alpha \mathbf{j}_\alpha + \chi_E \nabla \left(\epsilon_0 \nabla \cdot \mathbf{E} - \sum_\alpha q_\alpha n_\alpha \right), \tag{59}$$

where χ_E is a constant electric field divergence error diffusivity.

The resulting parabolic equations reduce the divergence errors throughout the domain at any given moment. Specifically, the error is not moved from one region to

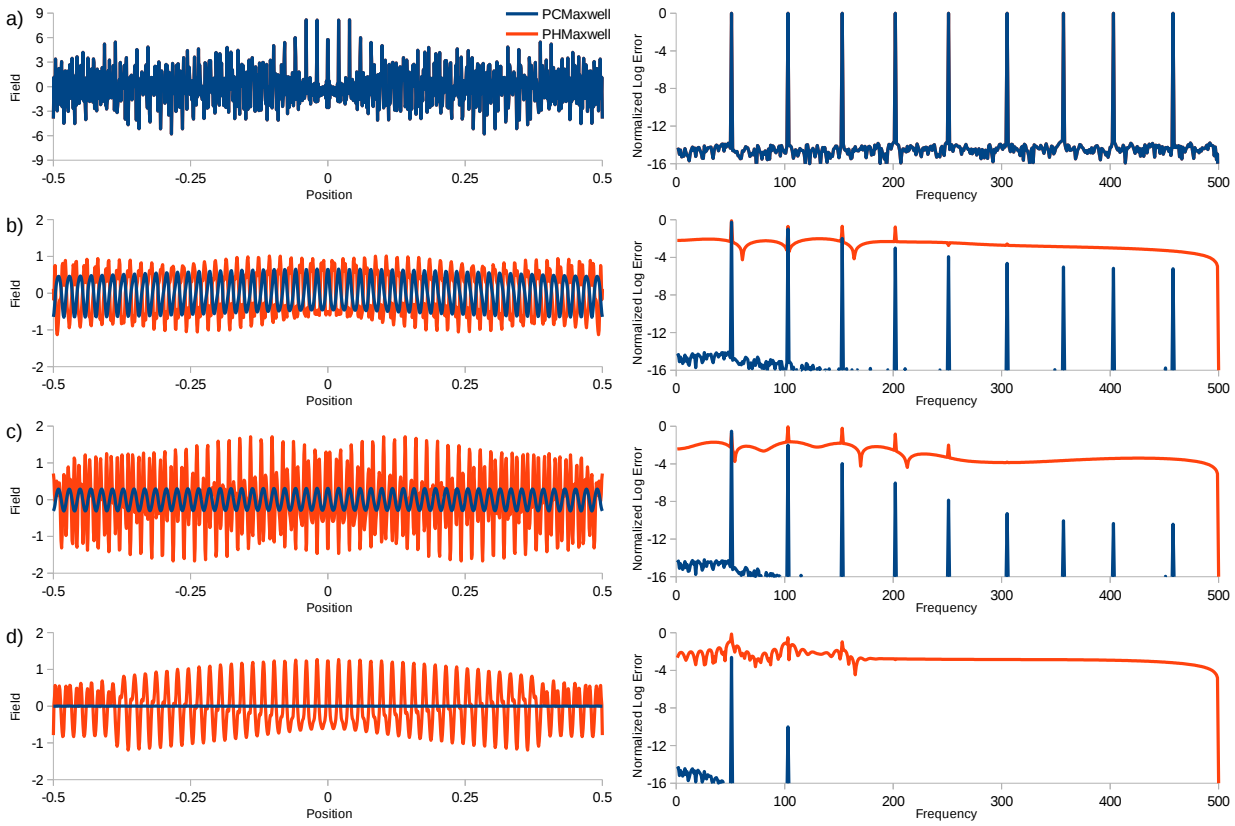

Figure 7: Divergence cleaning comparison between the parabolic (blue) and hyperbolic (red) methods. Left column shows the solutions at $t = 0$, 12, 24, 120. Right column shows the spatial frequency spectrum of the divergence error.

another as it is with the hyperbolic formulation. The diffusivities, χ_B and χ_E, can be set to convenient values to reduce the divergence errors to acceptable levels without overly restricting the time advance. Implicit formulations are also possible.

The parabolic cleaning method has been implemented in 1D to demonstrate its improved performance compared to the hyperbolic formulation. Figure 7 shows a comparison to the hyperbolic cleaning method. The spatial frequency content of the error demonstrates the local reduction of the parabolic cleaning method. The method monotonically removes the divergence error at all frequencies. The hyperbolic method leads to a broadband spectrum with less error reduction.

1.7.5 Open Boundary Conditions

The continuum kinetic and multi-fluid plasma models have waves with disparate speeds – from fast light waves to slow ion acoustic waves. Plasma simulations typically have

timescales of interest that are much longer than the transit times of the fastest waves across the computational domain. If the simulation is modeling an unbounded region, these wave should leave the computational domain without reflection. However, many numerical treatments for open boundary conditions generate non-physical reflections which contaminate the solution. We have implemented non-local boundary conditions that use a lacuna-based method [63] where an overlapping auxiliary domain is appended to the interior domain and the boundary condition is replaced with an interface condition.

The governing equation in the interior domain is expressed as

$$\frac{\partial}{\partial t}q + \frac{\partial}{\partial x_k}F_k(q) = S(q), \tag{60}$$

like Eq. (4), where α has been dropped for clarity. In the auxiliary domain the governing equation is defined as

$$\frac{\partial}{\partial t}w + \frac{\partial}{\partial x_k}F_k(w) = S(w) + \Omega(q), \tag{61}$$

where $\Omega(q)$ is the "near-boundary source". The solutions are matched in a transition region, so $w = q\mu(\mathbf{x})$. The smooth function $\mu(\mathbf{x})$ is zero at the beginning of the auxiliary domain and one at the interior/exterior interface. The boundary condition for the interior solution is then set such that the interface condition is

$$q\Big|^{-}_{interface} = w\Big|^{+}_{interface}. \tag{62}$$

The auxiliary solution is periodically re-integrated to damp the leading edge of the solution before it reflects and contaminates the interior solution.

We have successfully implemented advanced methods for numerically treating open boundaries in Refs. [47, 48]. The lacuna-based method works for oblique incidence waves in either purely hyperbolic or mixed hyperbolic/parabolic systems. The method even works in two dimensions where there is no true lacuna. (Huygens' principle states true lacunae only exist in odd dimensional space.) Sample results are shown in Fig. 8 where a pressure pulse interacts with open boundaries on all sides with a high extinction rate of the reflected wave.

2 Project Personnel

This project was performed by Prof. Uri Shumlak and graduate students Eric Meier, Andrew Ho, Robert Lilly, Sean Miller, Noah Reddell, Eder Sousa, and Bhuvana Srinivasan. Archival journal and conference papers were published reporting on the work from this project:

- G.V. Vogman, P. Colella, and U. Shumlak. "Dory-Guest-Harris instability as a benchmark for continuum kinetic Vlasov-Poisson simulations of magnetized plasmas." *Journal of Computational Physics* **277**, 101-120 (2014).

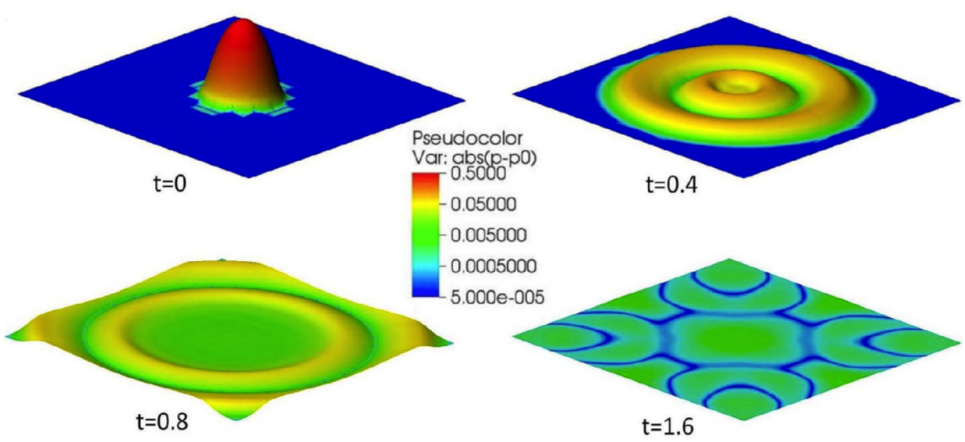

Figure 8: Lacuna-based open boundaries interact with a cylindrically expanding pressure pulse and exhibits a high extinction rate of the reflected wave.

- E. Kansa, U. Shumlak, and S. Tsynkov. "Discrete Calderon's projections on parallelepipeds and their application to computing exterior magnetic fields for FRC plasmas." *Journal of Computational Physics* **234**, 172-198 (2013).
- E.T. Meier and U. Shumlak. "A general nonlinear fluid model for reacting plasma-neutral mixtures." *Physics of Plasmas* **19**(7), 072508 (2012).
- E.T. Meier, A.H. Glasser, V.S. Lukin, and U. Shumlak. "Modeling open boundaries in dissipative MHD simulations." *Journal of Computational Physics* **231**(7), 2963-2976 (2012)
- U. Shumlak, R. Lilly, N. Reddell, E. Sousa, and B. Srinivasan, "Advanced physics calculations using a multi-fluid plasma model." *Computer Physics Communications* **182**, 1767-1770 (2011).
- B. Srinivasan and U. Shumlak. "Analytical and computational study of the ideal full two-fluid plasma model and asymptotic approximations for Hall-magnetohydrodynamics." *Physics of Plasmas* **18**(9), 092113 (2011).
- B. Srinivasan, A. Hakim, and U. Shumlak, "Numerical methods for two-fluid dispersive fast MHD phenomena." *Communications in Computational Physics* **10**(3), 183-215 (2011).
- J. Loverich, A. Hakim, and U. Shumlak, "A discontinuous Galerkin method for ideal two-fluid plasma equations." *Communications in Computational Physics* **9**, 240-268 (2011).

Dissertations and theses can be obtained from the University of Washington library system or from the project website, http://www.aa.washington.edu/research/cpdlab/.

Archival publications can be downloaded from ResearchGate.

3 Conclusions

Investigating advanced plasma models is motivated by the need to simulate complicated plasma physics phenomena that is not captured in simpler models. The multi-fluid plasma model is proving to be a model that is significantly more advanced and complete than the usual MHD model. Developing numerical algorithms to solve these more complete plasma models that exploit the different physics offers computationally efficient methods that maintain high order spatial accuracy. The methods extend to other continuum desriptions, such as continuum kinetic plasma model and single-fluid MHD models. The algorithm developed in the project, its implementation into WARPX, and its application to benchmark and real experimental problems have demonstrated the capability of both the multi-fluid plasma model and the numerical techniques in the algorithm.

Acknowledgment/Disclaimer

This work was sponsored by the Air Force Office of Scientific Research, USAF, under grant number FA9550-11-1-0167. The views and conclusions contained herein are those of the author and should not be interpreted as necessarily representing the official policies or endorsements, either expressed or implied, of the Air Force Office of Scientific Research or the U. S. Government.

References

[1] R. E. Peterkin Jr., M. H. Frese, and C. R. Sovinec. Transport of Magnetic Flux in an Arbitrary Coordinate ALE Code. *Journal of Computational Physics*, 140(1):148–171, Feb 1998.

[2] O. S. Jones, U. Shumlak, and D. S. Eberhardt. An implicit scheme for nonideal magnetohydrodynamics. *Journal of Computational Physics*, 130(2):231 – 242, 1997.

[3] D. Bonfiglio, S. Cappello, R. Piovan, L. Zanotto, and M. Zuin. 3d nonlinear mhd simulations of ultra-low q plasmas. *Nuclear Fusion*, 48(11):115010, 2008.

[4] S. Fromang and J. Papaloizou. MHD simulations of the magnetorotational instability in a shearing box with zero net flux. *Astronomy and Astrophysics*, 476(3):1113–1122, 2007.

[5] V. A. Izzo, D. G. Whyte, R. S. Granetz, P. B. Parks, E. M. Hollmann, L. L. Lao, and J. C. Wesley. Magnetohydrodynamic simulations of massive gas injection into Alcator C-Mod and DIII-D plasmas. *Physics of Plasmas*, 15(5), May 2008.

[6] M. Selwa, S. K. Solanki, K. Murawski, T. J. Wang, and U. Shumlak. Numerical simulations of impulsively generated vertical oscillations in a solar coronal arcade loop. *Astronomy and Astrophysics*, 454:653–661, Aug 2006.

[7] C. Z. Cheng and Georg Knorr. The Integration of the Vlasov Equation in Configuration Space. *Journal of Computational Physics*, 22(3):330–351, 1976.

[8] H Ruhl and P Mulser. Relativistic Vlasov Simulation of Intense Fs Laser Pulse-Matter Interaction. *Physics Letters A*, 205(5-6):388–392, 1995.

[9] L. Chacon, D. C. Barnes, D. A. Knoll, and G. H. Miley. An implicit energy-conservative 2D Fokker-Planck algorithm. *Journal of Computational Physics*, 157(2):618–653, 2000.

[10] L. Chacon, D. C. Barnes, D. A. Knoll, and G. H. Miley. An implicit energy-conservative 2D Fokker-Planck algorithm - II. Jacobian-free Newton-Krylov solver. *Journal of Computational Physics*, 157(2):654–682, 2000.

[11] Y. Matsunaga, T. Hatori, and T. Kato. Kinetic simulation of nonlinear phenomena of an ion acoustic wave in gas discharge plasma with convective scheme. *Physics of Plasmas*, 8(3):1057–1069, 2001.

[12] M. H. L. van der Velden, W. J. M. Brok, J. J. A. M. van der Mullen, and V. Banine. Kinetic simulation of an extreme ultraviolet radiation driven plasma near a multilayer mirror. *Journal of Applied Physics*, 100(7):073303, 2006.

[13] Sanae-I Itoh and Kimitaka Itoh. Kinetic Description of Nonlinear Plasma Turbulence. *Journal Of The Physical Society Of Japan*, 78(12):124502, 2009.

[14] M. J. Keskinen. Fully Kinetic Fokker-Planck Model of Thermal Smoothing in Nonuniform Laser-Target Interactions. *Physical Review Letters*, 103(5):055001, 2009.

[15] D. Loffhagen and F. Sigeneger. Advances in Boltzmann equation based modeling of discharge plasmas. *Plasma Sources Science & Technology*, 18(3):034006, 2009.

[16] V. Guerra, K. Kutasi, M. Lino da Silva, P. A. Sa, and J. Loureiro. Kinetic Simulation of Discharges and After-Glows in Molecular Gases. *High Temperature Material Processes*, 14(1-2):141–156, 2010.

[17] C. K. Birdsall and A. B. Langdon. *Plasma Physics via Computer Simulation*. McGraw-Hill, New York, 1985.

[18] Zhang-Hu Hu, Yuan-Hong Song, and You-Nian Wang. Wake effect and stopping power for a charged ion moving in magnetized two-component plasmas: Two-dimensional particle-in-cell simulation. *Physical Review E*, 82(2-1):026404, 2010.

[19] C. Soria-Hoyo, F. Pontiga, and A. Castellanos. A PIC based procedure for the integration of multiple time scale problems in gas discharge physics. *Journal of Computational Physics*, 228(4):1017–1029, 2009.

[20] A. Stockem, M. E. Dieckmann, and R. Schlickeiser. PIC simulations of the temperature anisotropy-driven Weibel instability: analysing the perpendicular mode. *Plasma Physics And Controlled Fusion*, 52(8):085009, 2010.

[21] S. E. Parker and W. W. Lee. A fully nonlinear characteristic method for gyrokinetic simulation. *Physics of Fluids B - Plasma Physics*, 5(1):77–86, 1993.

[22] U. Shumlak and J. Loverich. Approximate Riemann solver for the two-fluid plasma model. *Journal of Computational Physics*, 187(2):620–638, 2003.

[23] Jeffrey P. Freidberg. *Ideal Magnetohydrodynamics*. Plenum Press, New York and London, 1987.

[24] S. I. Braginskii. Transport processes in a plasma. In M. A. Leontovich, editor, *Reviews of Plasma Physics*, volume 1, pages 205–311. Consultants Bureau, New York, NY, 1965.

[25] S. Chapman and T. G. Cowling. *The Mathematical Theory of Non-Uniform Gases*. Cambridge University Press, Cambridge, 1939.

[26] J. D. Ramshaw. A Method for Enforcing the Solenoidal Condition on Magnetic Field in Numerical Calculations. *Journal of Computational Physics*, 52(3):592–596, 1983.

[27] C. D. Munz, P. Ommes, and R. Schneider. A three-dimensional finite volume solver for the Maxwell equations with divergence cleaning on unstructured meshes. *Computer Physics Communications*, 130:83–117, 2000.

[28] B. Marder. A method for incorporating Gauss' law into electromagnetic PIC codes. *Journal of Computational Physics*, 68(1):48–55, 1987.

[29] Jeong-Young Ji and Eric D. Held. Exact linearized Coulomb collision operator in the moment expansion. *Physics of Plasmas*, 13(10):102103, 2006.

[30] P. J. Catto. A short mean-free path, coupled neutral-ion transport description of a tokamak edge plasma. *Physics of Plasmas*, 1(6):1936–1943, 1994.

[31] H. Grad. On the Kinetic Theory of Rarefied Gases. *Communications On Pure And Applied Mathematics*, 2(4):331–407, 1949.

[32] Manuel Torrilhon. Hyperbolic Moment Equations in Kinetic Gas Theory Based on Multi-Variate Pearson-IV-Distributions. *Communications in Computational Physics*, 7(4):639–673, 2010.

[33] V. M. Zhdanov and G. A. Tirskii. The use of the moment method to derive the gas and plasma transport equations with transport coefficients in higher-order approximations. *PMM Journal of Applied Mathematics and Mechanics*, 67(3):365–388, 2003.

[34] R. Lilly and U. Shumlak. Comparisons of the two-fluid, ten moment and the two-fluid, five moment plasma models. *Bulletin of the American Physical Society*, 53(14), 2008.

[35] R. Lilly and U. Shumlak. Regions of validity for the 10-moment, two fluid plasma model. *DoD HPCMP Users Group Conference, 2008. DOD HPCMP UGC*, pages 150–153, 2008.

[36] Ammar Hakim. Extended MHD modeling with the ten-moment equations. *Journal of Fusion Energy*, 27(1-2):36–43, 2008.

[37] E. T. Meier, V. S. Lukin, and U. Shumlak. Spectral element spatial discretization error in solving highly anisotropic heat conduction equation. *Computer Physics Communications*, 181(5):837–841, 2010.

[38] A. Hakim, J. Loverich, and U. Shumlak. A high resolution wave propagation scheme for ideal two-fluid plasma equations. *Journal of Computational Physics*, 219(1):418 – 442, 2006.

[39] J. Loverich and U. Shumlak. A discontinuous Galerkin method for the full two-fluid plasma model. *Computer Physics Communications*, 169(1-3):251–255, 2005.

[40] J. Loverich, A. Hakim, and U. Shumlak. A discontinuous Galerkin method for ideal two-fluid plasma equations. *Communications in Computational Physics*, 9:240–268, 2011.

[41] U. Shumlak, R. Lilly, N. Reddell, E. Sousa, and B. Srinivasan. Advanced physics calculations using a multi-fluid plasma model. *Computer Physics Communications*, 182(9):1767–1770, 2011.

[42] B. Srinivasan, A. Hakim, and U. Shumlak. Numerical methods for two-fluid dispersive fast MHD phenomena. *Communications in Computational Physics*, 10:183–215, 2011.

[43] S. Miller and U. Shumlak. Validity and numerical implementation of the 13 moment multi-fluid plasma model. *Bulletin of the American Physical Society*, 58(16), 2013.

[44] A. Hakim and U. Shumlak. Two-fluid physics and field-reversed configurations. *Physics of Plasmas*, 14(5):055911, 2007.

[45] J. Loverich and U. Shumlak. Nonlinear full two-fluid study of $m = 0$ sausage instabilities in an axisymmetric Z pinch. *Physics of Plasmas*, 13(8):082310, 2006.

[46] B. Srinivasan and U. Shumlak. Analytical and computational study of the ideal full two-fluid plasma model and asymptotic approximations for Hall-magnetohydrodynamics. *Physics of Plasmas*, 18(9):092113, 2011.

[47] E. T. Meier, A. H. Glasser, V. S. Lukin, and U. Shumlak. Modeling open boundaries in dissipative MHD simulation. *Journal of Computational Physics*, 231(7):2963 – 2976, 2012.

[48] E. Kansa, U. Shumlak, and S. Tsynkov. Discrete Calderon's projections on parallelepipeds and their application to computing exterior magnetic fields for FRC plasmas. *Journal of Computational Physics*, 234(0):172–198, 2013.

[49] B. Cockburn and C. W. Shu. TVB Runge-Kutta Local Projection Discontinuous Galerkin Finite-Element Method For Conservation-Laws. *Mathematics Of Computation*, 52(186):411–435, 1989.

[50] B. Cockburn, S. C. Hou, and C. W. Shu. The Runge-Kutta Local Projection Discontinuous Galerkin Finite-Element Method For Conservation-Laws. *Mathematics Of Computation*, 54(190):545–581, 1990.

[51] B. Cockburn and C. W. Shu. The Runge-Kutta discontinuous Galerkin method for conservation laws. *Journal of Computational Physics*, 141(2):199–224, 1998.

[52] P. L. Roe. Approximate Riemann solvers, parameter vectors and difference schemes. *Journal of Computational Physics*, 43:357, 1981.

[53] Chi-Wang Shu and Stanley Osher. Efficient implementation of essentially non-oscillatory shock-capturing schemes. *Journal of Computational Physics*, 77(2):439–471, 1988.

[54] M. Brio and C. C. Wu. An upwind differencing scheme for the equations of ideal magnetohydrodynamics. *Journal of Computational Physics*, 75:400, 1988.

[55] Andrew L. Zachary and Phillip Colella. A higher-order Godunov method for the equations of ideal magnetohydrodynamics. *Journal of Computational Physics*, 99(2):341 – 347, 1992.

[56] J. Birn, J. F. Drake, M. A. Shay, B. N. Rogers, R. E. Denton, M. Hesse, M. Kuznetsova, Z. W. Ma, A. Bhattacharjee, A. Otto, and P. L. Pritchett. Geospace Environmental Modeling (GEM) Magnetic Reconnection Challenge. *Journal of Geophysical Research*, 106(2):3715, 2001.

[57] E. T. Meier and U. Shumlak. A general nonlinear fluid model for reacting plasma-neutral mixtures. *Physics of Plasmas*, 19(7):072508, 2012.

[58] R. Lilly and U. Shumlak. Multidimensional plasma sheath modeling using the three fluid plasma model in general geometries. *Bulletin of the American Physical Society*, 56(16), 2011.

[59] James A. Rossmanith and David C. Seal. A positivity-preserving high-order semi-Lagrangian discontinuous Galerkin scheme for the Vlasov-Poisson equations. *Journal of Computational Physics*, 230(16):6203–6232, 2011.

[60] R. E. Heath, I. M. Gamba, P. J. Morrison, and C. Michler. A discontinuous galerkin method for the vlasov–poisson system. *Journal of Computational Physics*, 231(4):1140 – 1174, 2012.

[61] Jing-Mei Qiu and Andrew Christlieb. A conservative high order semi-Lagrangian WENO method for the Vlasov equation. *Journal of Computational Physics*, 229(4):1130 – 1149, 2010.

[62] G.V. Vogman, P. Colella, and U. Shumlak. Dory–Guest–Harris instability as a benchmark for continuum kinetic Vlasov–Poisson simulations of magnetized plasmas. *Journal of Computational Physics*, 277(0):101 – 120, 2014.

[63] S.V. Tsynkov. On the application of lacunae-based methods to maxwell's equations. *Journal of Computational Physics*, 199(1):126 – 149, 2004.